ORIGINAL PAPER

CRET-based immunoassay on magnetic beads for selective and sensitive detection of Nanog antigen as a key cancer stem cell marker

Fatemeh Mehrabi[1] · Bijan Ranjbar[1,2] · Morteza Hosseini[3] · Niloufar Sadeghi[4] · Javad Mohammadi[5] · Mohammad Reza Ganjali[6]

Abstract

A method is presented for chemiluminescence resonance energy transfer (CRET) using APTES-Fe_3O_4 as a highly efficient energy acceptor with strong magnetic effectiveness over extended distances, while an Au@BSA-luminol composite acts as the donor. In order to boost the chemiluminescence reactions, CuO nanoparticles were successfully employed. The distance between the donor and acceptor is a crucial factor in the occurrence of the CRET phenomenon. A sensitive and high-throughput sandwich chemiluminescence immunosensor has been developed accordingly with a linear range of 1.0×10^{-7} g/L to 6.0×10^{-5} g/L and a limit of detection of 0.8×10^{-7} g/L. The CRET-based sandwich immunosensor has the potential to be implemented to early cancer diagnosis because of its high sensitivity in detecting Nanog, fast analysis (30 min), and simplicity. Furthermore, this approach has the potential to be adapted for the recognition of other antigen–antibody immune complexes by utilizing the corresponding antigens and their selective antibodies.

Keywords Chemiluminescence resonance energy transfer (CRET) · Nanog · Sandwich immunosensor · Au@BSA-luminol · APTES-Fe_3O_4

✉ Bijan Ranjbar
ranjbarb@modares.ac.ir

✉ Morteza Hosseini
Hosseini_m@ut.ac.ir

[1] Department of Nanobiotechnology, Faculty of Biological Sciences, Tarbiat Modares University, Tehran, Iran

[2] Department of Biophysics, Faculty of Biological Sciences, Tarbiat Modares University, Tehran, Iran

[3] Nanobiosensors Lab, Department of Life Science Engineering, Faculty of New Sciences & Technologies, University of Tehran, Tehran 1439817435, Iran

[4] Medical Genetics Department, Institute of Medical Biotechnology (IMB), National Institute of Genetic Engineering and Biotechnology (NIGEB), Tehran, Iran

[5] Department of Life Science Engineering, Faculty of New Sciences & Technologies, University of Tehran, Tehran 1439817435, Iran

[6] Center of Excellence in Electrochemistry, School of Chemistry, College of Science, University of Tehran, Tehran 1439817435, Iran

Introduction

Non-radiative (dipole–dipole) energy transfer between a luminescent doner and acceptor is the basis of resonance energy transfer (RET) [1]. These processes are generally categorized as fluorescence RET (FRET), bioluminescence RET (BRET), or chemiluminescence RET (CRET), depending on the nature of the donor (either a fluorophore, bioluminescent protein, or chemiluminescent compound) [2]. The distance between the donor and acceptor plays a crucial role in facilitating chemiluminescent resonance energy transfer (CRET) [3]. CRET-based assays demonstrate high sensitivity and the absence of an external excitation by light results in low background noise of these assays. During the past few decades, there has been increasing focus on chemiluminescence immunoassay (CLIA) as an analytical technique across various fields such as environmental [4], clinical [5], pharmaceutical [6], food [7], and agricultural [8] analysis. This is primarily due to the exceptional sensitivity, ease of use, and broad linear range of these methods [9].

Nanog Homeobox is a gene with a significant role in the maintenance of pluripotency in embryonic stem cells

[10]. It is a key transcription factor that helps regulate gene expression pertaining to cell differentiation and self-renewal. Nanog Homeobox is imperative in keeping stem cells in the undifferentiated state and is considered a master regulator of pluripotency. Nanog is the product of the *nanog* gene situated on chromosome 12 which consists of four exons and three introns [11, 12]. The human Nanog protein is comprised of 305 amino acids with a homeodomain. The estimated molecular weight of Nanog is around 35 kDa [13]. Recent research has established a connection between elevated levels of Nanog in different types of cancers and the regulation of various molecules. This reciprocal relationship has been proven to contribute to the promotion of proliferation, metastasis, invasion, and chemoresistance. Consequently, Nanog acts as an oncogene by inducing stem cell circuitries and fostering heterogeneity within cancer cells [14]. Cancer stem cells (CSCs) or tumor-initiating cells, based on the type of cancer, exhibit varying levels of expression of transcription factors. Elevated levels of these stemness genes are seen in CSCs across various tumor types, playing a crucial role in sustaining the stem cell program [15].

Developing CRET-based detection systems have pivoted around nanomaterials in the recent years including magnetic iron oxide nanoparticles (MNPs), gold nanoparticles (AuNPs) and copper oxide nanoparticles (CuONPs) as the carriers, donors or acceptors [16–19] and enhancers [20]. Studies have explored the use of magnetic beads (MBs) for developing immunoassays based on CRET for the detection of antigens [21].

Herein, a CRET-based immunoassay using MBs for the detection of Nanog was developed. For the first time, CRET-based (3-aminopropyl) triethoxysilane (APTES)-Fe3O4 nanoparticles and luminol/H_2O_2/CuONPs were fabricated for the sensitive detection of Nanog antigen. The CRET phenomenon was triggered by close proximity of the Au@BSA-luminol-Ab$_2$ (Nanog antibody) nanocomposites, as the chemiluminescence (CL) light source, and the APTES-Fe3O4-Ab$_1$ (Nanog antibody) in immune complexes formed on the MBs surface, which activates the luminescence of APTES-Fe$_3$O$_4$. The APTES compound is a crucial silane coupling agent extensively employed as a grafting agent to enhance the interfacial behavior of various inorganic oxides such as silica, ceramics, titania, and magnetic iron oxide nanoparticles (MNPs) [22]. MNPs with APTES surface functionalization have particularly been prominent in many biological applications involving antibodies [23]. A less mentioned feature for APTES is its intrinsic fluorescence property [24]. Absorption and emission spectrum studies for APTES and APTES-Fe$_3$O$_4$ showed that not only APTES has intrinsic fluorescence emission, but also the APTES-Fe$_3$O$_4$ nanoparticles have absorption and fluorescence emission. The interaction of APTES with Fe$_3$O$_4$ nanocrystals

was assessed by investigating the absorption and emission spectra. The overlap of the absorption spectrum of APTES-Fe$_3$O$_4$NPs with the emission spectrum of luminol-H_2O_2 led to design a CRET-based diagnostic system.

The CRET energy transfer distance between the donor (Au@BSA-luminol-Ab$_2$-H_2O_2-CuONPs CL system) and acceptor (APTES-Fe$_3$O$_4$NPs-Ab$_1$) occurs after the sandwich immunocomplex is formed. The Au@BSA nanoparticles have numerous binding sites to accommodate a large number of Ab binding, and they also demonstrate a strong adsorption capacity for luminol molecules. The immunocomplex formation between the antigen (Ag) and the carboxyl-modified APTES-Fe$_3$O$_4$ antibody in the presence of Au@BSA-luminol-Ab$_2$ after magnetic separation was the basis of the determination step. CuONPs acts as the oxidation catalyzer of luminol by H_2O_2 to yield CL. CuONPs are highly stable and exhibit strong peroxidase-like activity with consistent catalysis under various pH and temperature conditions [25]. CuONPs have been known to highly enhance the CL intensity in luminol-H_2O_2 systems [26]. Nanog detection was carried out based on the sensitive CL immunoassay using APTES-Fe$_3$O$_4$, luminol and nanomaterials conjugates. Therefore, the target Nanog was sensitively and selectively detected.

Experimental section

Chemicals and materials

1-(3-dimethylaminopropyl)-3-ethylcarbodiimide hydrochloride (EDC), N-hydroxysuccinimide (NHS), and bovine serum albumin (BSA), PBS buffer (0.1 M, pH 7.4), 3-aminopropyltriethoxysilane (APTES)99%, Ferrous chloridetetrahydrate (FeCl$_2$.4H$_2$O), ammonium hydroxide (NH$_4$OH), copper (II)chloride hexahydrate (Cl$_2$CuH$_{12}$O$_6$), gold (III) chloride hydrate (HAuCl$_4$·4H$_2$O, 99%), luminol (C$_8$H$_7$N$_3$O$_2$) and hydrogen peroxide (H$_2$O$_2$) were attained from Sigma Aldrich. Sodium citrate, glacial acetic acid(C$_2$H$_4$O$_2$), sodium borohydride (NaBH$_4$), and glutaraldehyde (25%) (GA) were purchased from Merck Chemical Co.

The monoclonal antibody anti-Nanog (made in rabbit, 1.3 g/L) (Ab$_1$ and Ab$_2$), and Nanog antigen (Nanog Ag), human epidermal growth factor receptor 2 (HER2), receptor tyrosine kinase-like orphan receptor 1 (ROR1) and prostate-specific antigen (PSA) were attained from Padzacompany (Iran). PBS buffer (0.1 M buffer, pH 7.4) was used for the preparation and dilution of antigens and antibodies.

Apparatus

A LS-55 luminescence spectrometer (Perkin-Elmer, USA) was used for CL spectra measurement. Absorption spectra

were acquired using a Perkin Elmer lambda25 spectrometer. The UV–visible spectra were attained using a Perkin Elmer Lambda 35 spectrophotometer. AuNPs were characterized using a transmission electron microscope (TEM) (Zeiss, EM10C, 80 kV, Germany). The TEM samples were prepared by letting a drop of a colloidal solution dry at room temperature on carbon-coated copper grid. A Field emission scanning electron microscope (FE-SEM) (TESCAN, MIRA3, Czech) was used to observe the morphology of the APTES-Fe_3O_4 nanoparticles samples.

Preparation of Au@BSA nanomaterials and synthesis of luminol and Ab$_2$ labeled Au@BSA (luminol-Au@BSA-Ab$_2$)

The synthesis process utilized AuNPs that were obtained using a previously published method, with small modifications [27–30]. Briefly, 5 mL trisodium citrate solution (38 mM) was mixed with a 25 mL boiling solution of $HAuCl_4$ (1 mM) under constant stirring. A color change to red wine was witnessed within about 8–10 min as a sign of the formation of the gold seeds [31, 32]. Following that, BSA was introduced which adhered to the NPs via thiol groups and led to the formation of functional groups. For this, sodium borohydride (6 mg) was used to denature a freshly prepared BSA solution (24 mg) and kept for overnight under vigorous stirring. This process reduces the disulfide bonds to generate thiol groups and also adds extra thiol groups onto the surface of BSA [33]. We thus centrifuged and washed the resulting product with double-distilled water and ethanol several times. All compounds were freeze-dried and stored at 4 ∘C until further use.

The chemical bonding approach was used to create the luminol and Ab$_2$ modified Au@BSA study. Via ultrasonication, we dissolved 2 mg of Au@BSA in 1 mL double-distilled water and thus mixed it with 400 µL of 12.5% GA. To ensure the adherence of GA to the Au@BSA surface, the resulting solution was shaken for 3 h. The unreacted chemicals were then removed by centrifugation and several washing steps from the GA-linked Au@BSA before being dissolved in 1 mL PBS (0.1 M, pH 7.4). The above solution was then mixed with a 0.1 M luminol solution shaken for 4 h. In order to activate the carboxylic groups on the surface of BSA, the generated Au@BSA-luminol nanocomposites underwent centrifugation and were then washed in 2 mL 0.1 M PBS (pH 7.4) which contained 2 mg EDC and 2 mg NHS with a 2 h shaking periods. Finally, 80 µL Ab$_2$ antibodies (1 g/L) was mixed with the solution and slowly stirred in an ice bath for 8 h to ensure the luminol-Au@BSA and Ab$_2$ conjugation. All remaining reagents were removed by centrifuging the resulting luminol-Au@BSA-Ab$_2$ nanocomposites at 6000 rpm and washing them with double-distilled water.

The resulting nanocomposites were ultimately dispersed in 2 mL PBS (0.1 M, pH 7.4) until further use.

Synthesis of APTES-Fe$_3$O$_4$ nanoparticles and preparation of antibody immobilized on MBs

In this method, $FeCl_2.4H_2O$ (0.3125 g) was dissolved in 10 mL DDW and stirred in order to attain a homogeneous mixture. Ammonia solution (25%) (1.6 mL) was mixed under constant stirring which enabled the oxidation of Fe (II). The solution was left to stir for 10 min. APTES (0.625 mL) was thus mixed and again the mixture was stirred for an extra 10 min. The reaction mixture was autoclaved in a 50 mL volume sealed pressure vessel at 134 °C for 3 h and then cooled at room temperature. This resulted in black precipitates, which were purified through several washing steps with water and ethanol to ensure the elimination of excess reactants. Magnetic separation was used for the final separation of the resulting compound which was dried at 80 °C for 7–8 h using a hot air oven [22]. Surface functionalization of the MNPs was carried out to generate amine groups (-NH2) on their surface for their covalent bonding to carboxyl groups (-COOH) on the antibodies. Accordingly, APTES-Fe_3O_4 was used. Covalent coupling of the antibody to the amino-functionalized MNPs was carried out based on the classical EDC/NHS blocking chemistry [34]. Briefly, to activate the antibody, NHS (9 mg) and EDC (5 mg) were dissolved in 1 mL PBS buffer (0.1 M, pH 7.4) and added to MNPs (1 mL, 0.1 g/L) in PBS (0.1 M, pH 7.4). Finally, we introduced 80 µL of Nanog antibodies (1 g/L) to the mixture which was stirred slowly in an ice bath for 8 h for the effective attachment of the Ab$_2$ to the surface of the APTES-Fe_3O_4 [35].

Synthesis of cupric oxide nanoparticles

The sol–gel method was implemented for the synthesis of the CuO nanopowders. In a sterile round bottom flask, an aqueous solution of $CuCl_2.6H_2O$ (0.2 M) was first prepared; 1 mL of glacial acetic acid was introduced to the prepared solution and thus heated to 100 ℃ under continuous stirring. In order to attain a pH of 7, 8 M of NaOH solution was added. This resulted in the immediate color change from blue to black and the formation of large amounts of black precipitate at the bottom of the flask. The precipitates were gathered through centrifugation and washed 3–4 times with deionized water. The obtained precipitates were then dried in air for 24 h [36].

Determination of Nanog

As shown in Scheme 1, a biosensing platform for Nanog Ag detection was developed using the CRET-based immunosensor. 200 µL of the Au@BSA-luminol-Ab$_2$ suspension
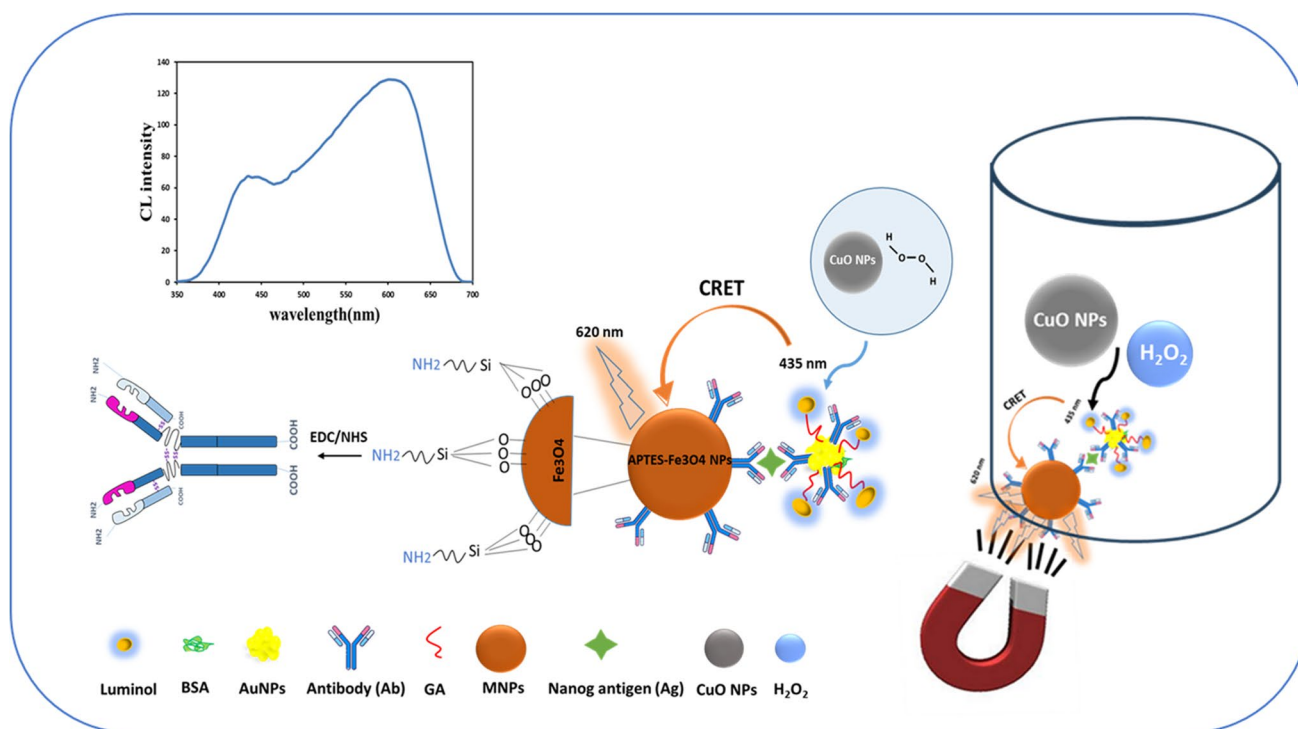
Scheme 1 Schematic illustration of the sandwich CL immunosensor based on CRET for the Nanog antigen assay

was mixed with 50 μL of 0.1×10^{-6} g/L Nanog solution, and the final mixture was incubated for 15 min in an ice bath to allow the Au@BSA-luminol-Ab_2-Nanog immune complexes to form. Then, a 200 μL volume of APTES-Fe_3O_4-Ab_1 was also mixed for 15 min in the ice bath. After that, we separated the suspension magnetically and resuspended it in 200 μL of PBS (0.1 M, pH 7.4). The final mixture was transferred to a 1 cm path length quartz cell. Then 50 μL of the CuONPs was added to the suspension, followed by the immediate introduction of H_2O_2 (1.0×10^{-3} M) to the quartz cell. The CL spectrum was recorded immediately with a LS-55 luminescence spectrometer.

Results and discussion

Characterization of Au@BSA nanoparticles

TEM was used to analyze the morphology and structure of the Au@BSA nanoparticles. As depicted in Fig. S1a, the nanoparticles exhibited spherical-shaped particles coated with a BSA layer with an average size of approximately 15 nm. The proposed immunosensor benefited from the presence of Au@BSA nanoparticles, which was made of several self-assembled Au nanoparticles. These nanoparticles exhibited a large surface area with high

electroconductivity, leading to enhanced electron transfer and improved assay sensitivity [37]. The BSA layer coating the Au@BSA nanoparticles provided a versatile platform, allowing for easy conjugation of a significant quantity of luminol and anti-Nanog antibodies. In this case, the beneficial functional groups (-COOH, -NH_2, and -SH) found on the external BSA layer facilitate the cross-linking of numerous Anti-Nanog and luminol molecules [38]. Our team's earlier publications (Hosseini et al. [39, 40]) have validated the satisfactory outcomes of Energy Dispersive Spectroscopy (EDS) for the subsequent assessment of the synthesized Au@BSA nanoparticles, which further confirmed the presence of gold, carbon, nitrogen, and oxygen elements corroborating the successful synthesis of the Au@BSA nanoparticles.

The FTIR spectrum, as depicted in Fig. S1b, displayed the common stretching vibrations of –OH resulting in the wide peaks at 3446 cm^{-1}, 3382 cm^{-1}, 3131 cm^{-1} and the -NH vibrations which translated to a peak at 1403 cm^{-1}. The absorption band at 2361 cm^{-1} can be assigned to alkyl groups [–(CH_2)–] which are characteristic of the organic coupling agent. Moreover, the characteristic peaks at 1702, 993 and 1135 cm^{-1} resulted from the –COO group vibrations, further showing the variety of functional groups provided by the synthesized Au@BSA@anti-Ab_2, including –COOH and –NH_2 groups.

Characterization of APTES-Fe$_3$O$_4$ nanoparticles

The UV–Visible spectrum of 1 g/L solutions of Fe$_3$O$_4$ NPs and APTES-Fe$_3$O$_4$ NPs was recorded and is shown in Fig. 1A. A peak was observed at 406 ± 0.88 nm for APTES-Fe$_3$O$_4$ NPs [25]. As these nanoparticles are magnetic in nature (Fig. S2), coating them with non-magnetic material, such as APTES, helps minimize the magnetic forces between the particles. Furthermore, to understand the structure of APTES-Fe$_3$O$_4$ NPs, FTIR spectrum was recorded (Fig. 1C), which confirmed the conjugation of the antibodies to the MNPs. Characteristic Fe–O bonds were seen at 524 cm^{-1} pertaining to stretching vibrations, and at 859 cm^{-1} showing the stretching of Fe–O–H. The vibrations of OH on the surface of Fe$_3$O$_4$ are corroborated at 1077 cm^{-1} and the peak at 1160 cm^{-1} indicated the asymmetric stretching vibrations of the Si–O groups. The other characteristic broad peak at 3200–3600 cm^{-1} can be assigned to hydroxyl and amine groups. At around 1650 cm^{-1} a peak is seen which depicts the C=O bond of the antibody amide I. The one at 1403 cm^{-1} shows the N–H bond of antibody amide II. The absorption band at 2438 cm^{-1} is due to alkyl groups [–(CH$_2$)–] that are characteristic of the organic coupling agent. The reaction of silane molecules on the surface of Fe$_3$O$_4$ nanoparticles and covalent attachment of the antibodies to the MNP surface is perfectly confirmed by the FTIR spectrum. FE-SEM was used to assess the surface morphology of APTES-Fe$_3$O$_4$ NPs which showed uniform shape (spherical) and size of the particles. The image of APTES-Fe$_3$O$_4$ NPs is shown in Fig. 1B.
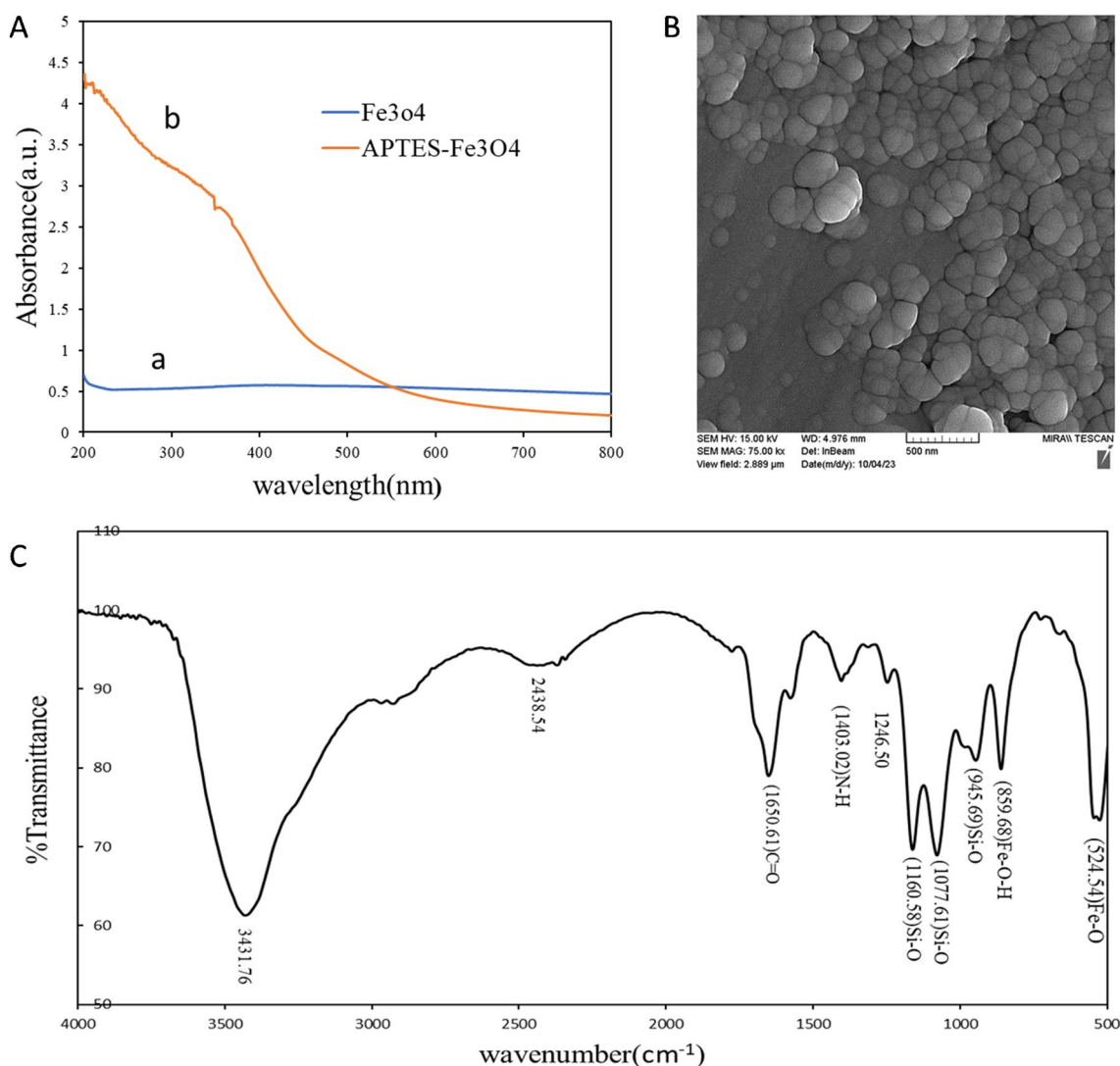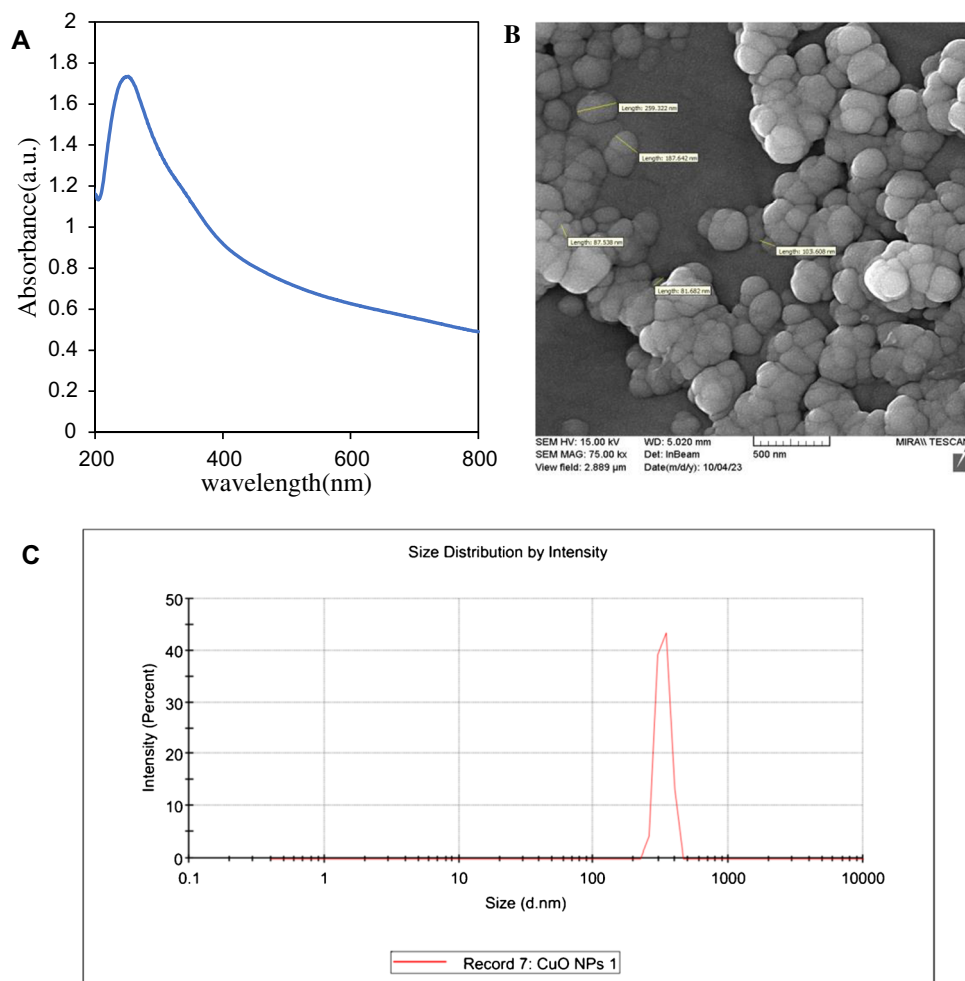

Fig. 1 **A** UV–visible absorption spectra of 1 g/L of Fe$_3$O$_4$ (a) and APTES-Fe$_3$O$_4$ (b); (**B**) FE-SEM of APTES-Fe$_3$O$_4$ nanoparticles; and (**C**) FTIR spectra of magnetic nanoparticles coated with silane (MNP) and conjugated with Anti-Nanog

Characterization of cupric oxide nanoparticles

Figure 2A displays the UV–Visible spectrum of 1 mM concentration solutions of CuO NPs. The size of the nanoparticles was estimated from the FE-SEM micrograph (Fig. 2B), revealing that the majority of the particles are less than 200 nm in size. These findings correlate with the data obtained from the particle size analyzer. The FE-SEM graph and Size Distribution Report by Intensity graph also illustrates that the copper oxide nanoparticles have a spherical shape and exhibit a nearly uniform size (Fig. 2C). The results display the relationship between intensity and Zeta Potential. It reveals a maximum value of -36.8 mV. The negative zeta potential indicates that the copper oxide particles are negatively charged and exhibit moderate stability [36, 41, 42]. The negative zeta potential of CuO nanoparticles prevents them from agglomerating, resulting in excellent dispersion stability. The well-dispersed and stable nature of CuO nanoparticles make them highly effective catalysts in chemical reactions. The catalytic properties of CuO have been tested in various chemical reactions, confirming its efficacy as a catalyst [43].

Optimization for the assay

In this work, CuONPs were used as an enhancer in the luminol-H_2O_2 CL system. The optimized CL reaction conditions and the assessment of the enhancing characteristics of CuONPs in the luminol-H_2O_2 CL system have been described. As depicted in Fig. S3, the best conditions for the luminol-H_2O_2-CuONPs CL system were 5.0 mM H_2O_2 aqueous solution (Fig. S3A) and 3.0×10^{-3} g/L CuONPs solution (Fig. S3B). Also, the optimal time for CL reaction was 6 s (Fig. S3C). In all experiments, the concentration of APTES-Fe_3O_4 remained constant at 1 g/L, with the addition of 200 μL of the Au@BSA-luminol-Ab_2 suspension.

CRET mechanism

The CRET-based immunoassay was constructed with luminol-H_2O_2, which acted as the donor and APTES-Fe_3O_4 as the acceptor. CRET was based on an immuno-interaction of Au@BSA-Ab_2 and APTES-Fe_3O_4-Ab_1 (anti-Nanog) in the H_2O_2 and CuONPs chemiluminescence reaction in the presence of target (Nanog Ag). When luminol-Au@BSA-Ab_2

Fig. 2 (**A**) UV–visible absorption spectrum of CuO NPs, 1 mM (PBS, pH 7.4); (**B**) FE-SEM image of CuO nanoparticles; and (**C**) Dynamic light scattering (DLS) measurements of size dispersion of CuONPs

is exposed to H_2O_2 and excited at 435 nm, the resulting excitation is weak. Therefore, the use of a catalyst, such as CuONPs, becomes necessary. The investigation focused on the catalytic effects of CuONPs on the luminol-H_2O_2 chemi-luminescent system. Figure S4 demonstrates that, in alkaline media, the oxidation of luminol by H_2O_2 produces a weak chemiluminescent (CL) signal. However, with the addition of CuO nanoparticles, the intensity of the CL signal can be significantly enhanced by approximately 13.0 folds.

The absorption and emission spectrum studies for APTES and APTES-Fe_3O_4 showed that APTES has intrinsic fluorescence emission (Fig. S5). The fluorescence spectrum and UV–visible of APTES-Fe_3O_4 NPs showed that these nanoparticles have luminescence emission in the range of 620 nm and absorption in the region of 435 nm (Fig. S6 and Fig. S7). The overlapping absorption spectrum of APTES-Fe_3O_4 NPs with the emission spectrum of luminol-H_2O_2 facilitated the design of a CRET-based diagnostic system (Fig. 3). To investigate the target detection capability of the biosensor, the complex was reacted with different concentrations of Nanog from 1.0×10^{-8} g/L to 6.0×10^{-5} g/L. There was a uniform increasing trend in the CRET intensity with increasing target concentration, indicating the detection capability of this platform (Fig. 4A). With regard to the obtained results, the regression equation is $y = 11.848x + 101.74$, and the determination coefficient $R^2 = 0.9767$ suggests a linear relationship between Nanog Ag concentration of 1.0×10^{-7}

g/L to 6.0×10^{-5} g/L and CL intensity and with the limit of detection for the assay was 0.8×10^{-7} g/L, which was calculated according to the Eq. 3 σ / m, where m represents the slope of the calibration curve and σ is the standard deviation of the blank samples, as shown in Fig. 4B. The CRET based immunosensor performance for antigen detection was compared in Table S1 with similar publications, which includes the limits of detection (LOD), linear dynamic range, and donor/acceptor information obtained from the literature [30–33].

Selectivity

The critical parameter of selectivity plays a significant role in evaluating the performance of luminescence immunosensors. To further explore the selectivity of the described sensing platform, we conducted additional investigations. Specifically, we examined the CRET responses of the probe antibody towards potential interfering antigens including HER2 and PSA and ROR1. Various potential interfering antigens such as HER2, PSA, and ROR1 were evaluated at a concentration of 200×10^{-6} g/L, while the concentration of Nanog was 10×10^{-6} g/L. Despite the 20-fold concentration of the interfering antigens, the overall signal intensity in the presence of Nanog antigen remained notably higher compared to the other antigens. Results showed that their CRET intensities were significantly lower when compared to
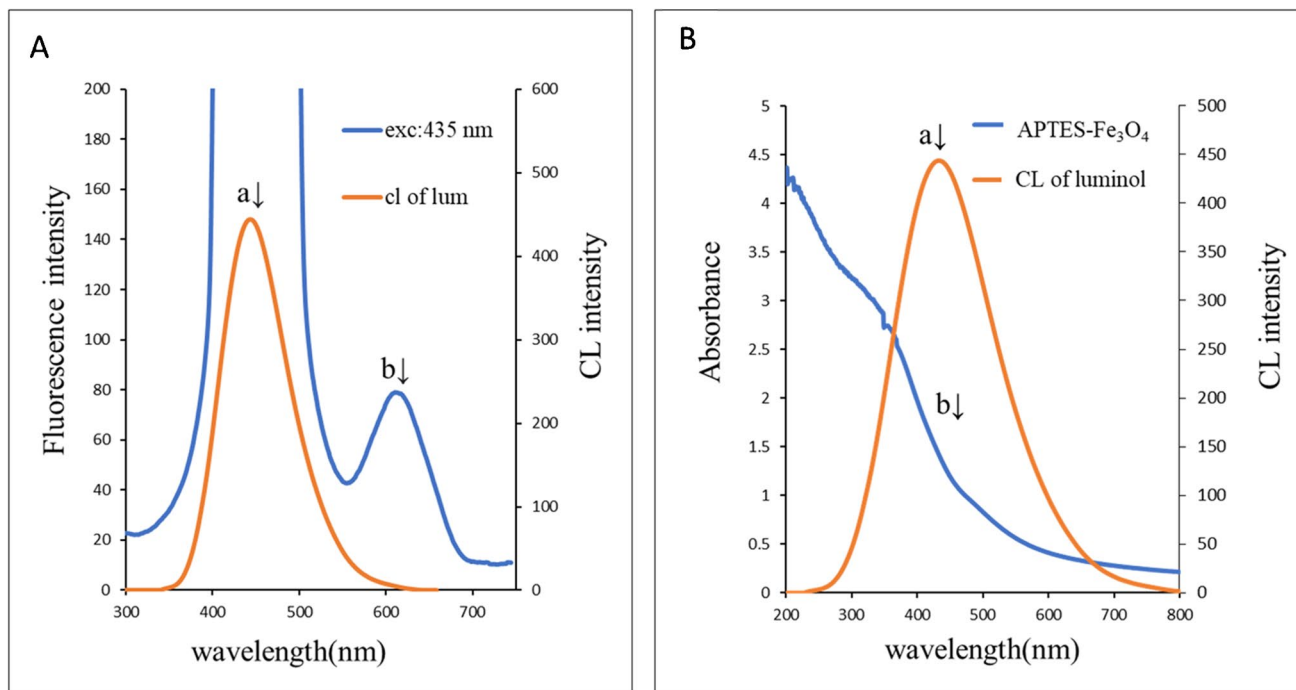

Fig. 3 A The overlapping fluorescence spectrum of APTES-Fe_3O_4 NPs with the emission spectrum of luminol-H_2O_2 (a) CL of luminol-H_2O_2 (b) fluorescence of APTES-Fe_3O_4 NPs at 435nm excitation

(PBS 0.1 M, pH 7.4); and **B**) The overlap of CL spectrum of luminol (a) and UV–visible absorption spectrum of APTES-Fe_3O_4 NPs (b)

Fig. 4 The in vitro detection of Nanog by CRET-based APTES-Fe$_3$O$_4$(MNPs): **A** CRET responses of Nanog at different concentrations; and (**B**) Linearity of CL signals versus Nanog concentrations (The concentration of Nanog was 0.1–60×10^{-6} g/L). Inset: plot of the CL intensity (the concentration of Nanog was 0.1–1.5×10^{-6} g/L)
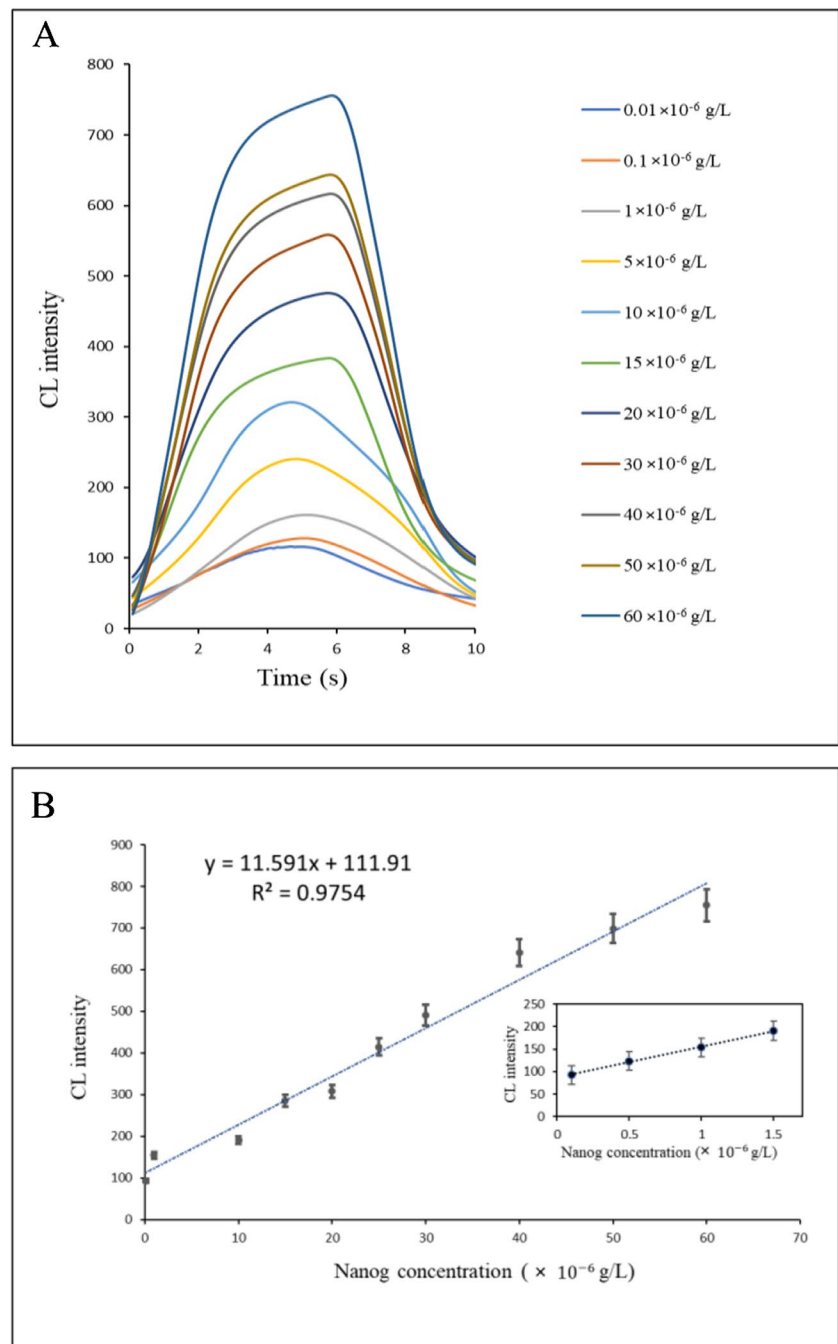
the Nanog sample, proving that the method was only specific for Nanog Ag (Fig. 5).

Performance test of the CRET-based immunoassay

The developed CRET-based immunoassay was employed to detect Nanog under ideal conditions. To better assess the analytical performance of the immunoassay system, a recovery test was conducted. To assess the analytical recovery, normal urine was spiked with a known concentration of Nanog and measured in 10 replicates within one analytical

run. Recovery and RSD for real samples varied from 103.5% to 106.4% and from 3.3% to 4.4%, respectively. This proves that the proposed method can effectively detect the target in biological samples.

Conclusions

In this study, a magnetic-based CRET immunoassay was developed for the detection of Nanog antigens. Notably, the acceptor itself serves as a magnetic component, offering a dual functionality. Nanog was chosen as a model analyte
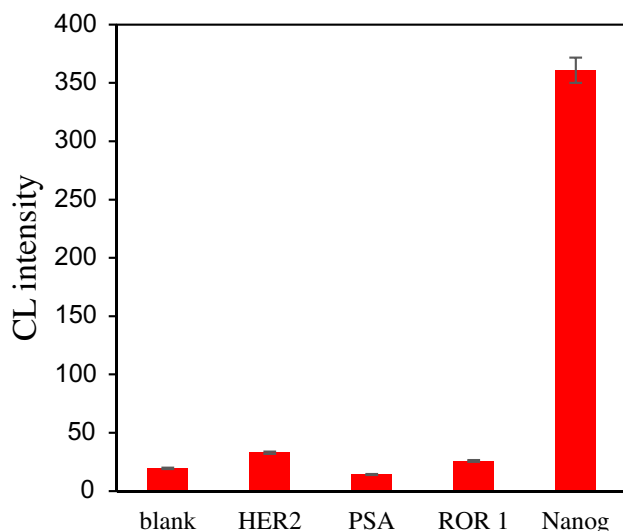
Fig. 5 The selectivity of the CRET-based immunoassay; the concentration of interfering antigens was 200×10^{-6} g/L and 10×10^{-6} g/L of Nanog. the concentration of H_2O_2 was 5.0×10^{-3} M; the concentration of CuONPs was 3.0×10^{-3} g/L

to depict the overall performance of the proposed strategy. Despite the requirement for magnetic separation, this method was remarkably time-efficient, with a measurement completion time of approximately 30 min, making it much faster and simpler than the conventional ELISA method. Additionally, this method demonstrated exceptional sensitivity, reaching ultrahigh levels.

Author contribution Fatemeh Mehrabi: Formal analysis, Visualization, Data curation, Writing-Original draft. **Bijan Ranjbar:** Conceptualization, Methodology, Designing the analysis, Writing-review & editing. **Morteza Hosseini:** Conceptualization, Methodology, Project administration, Funding acquisition, Writing-review & editing. **Niloufar Sadeghi:** Conceptualization, Methodology, Designing the analysis, Resource **Javad Mohammadi:** Methodology, writing-review & editing **Mohammad Reza Ganjali:** writing-review & editing.

All authors have given approval to the final version of the manuscript.

Data availability All data generated or analyzed during this study are included in this article and its supplementary information files.

Declarations

Ethical approval The work has been done in accordance with the recommendations of the National Institute of Genetic Engineering and Biotechnology (NIGEB) and the Human Ethical Committee of the University of Tarbiat Modares.

Conflicts of interests The authors declare no competing financial interests.

References

1. Jia BJ, He X, Cui PL, Liu JX, Wang JP (2019) Detection of chloramphenicol in meat with a chemiluminescence resonance energy transfer platform based on molecularly imprinted graphene. Anal Chim Acta 1063:136–143. https://doi.org/10.1016/j.aca.2019.02.044
2. Dou L, Pan Y, Ma M, Zhang S, Shen J, Wang Z, Yu W (2021) Antibody engineering-driven controllable chemiluminescence resonance energy transfer for immunoassay with tunable dynamic range. Anal Chim Acta 1152:338231. https://doi.org/10.1016/j.aca.2021.338231
3. Yan Y, Wang X, Hai X, Song W, Ding C, Cao J, Bi S (2020) Chemiluminescence resonance energy transfer: From mechanisms to analytical applications. TrAC Trends Anal Chem 123:115755
4. Gu L, Zou Y, Li Y, Zeng K, Zhu N, Zhu F (2020) High-throughput chemiluminescence immunoassay based on Co2+/hemin synergistic catalysis for sensitive detection tetrabromobisphenol A bis (2-hydroxyethyl) ether in the environments. Sci Total Environ 714:136880
5. Salvagno GL, Gianfilippi G, Fiorio G, Pighi L, De Nitto S, Henry BM, Lippi G (2021) Clinical assessment of the DiaSorin LIAISON SARS-CoV-2 Ag chemiluminescence immunoassay. Ejifcc 32(2):216
6. Franzin M, Ruoso R, Concato M, Radaelli D, D'Errico S, Addobbati R (2024) Applicability of a chemiluminescence immunoassay to screen postmortem bile specimens and its agreement with confirmation analysis. Int J Mol Sci 25(7):3825
7. Li ZB, Cui PL, Liu J, Liu JX, Wang JP (2020) Production of generic monoclonal antibody and development of chemiluminescence immunoassay for determination of 32 sulfonamides in chicken muscle. Food Chem 311:125966
8. Qiu Y, Li P, Liu B, Liu Y, Wang Y, Tao T, Xu J, Hammock BD, Liu X, Guan R, Zhang C (2019) Phage-displayed nanobody based double antibody sandwich chemiluminescent immunoassay for the detection of Cry2A toxin in cereals. Food Hydrocolloids 30(1):924–936
9. Chen J, Qiu H, Zhao S (2020) Fabrication of chemiluminescence resonance energy transfer platform based on nanomaterial and its application in optical sensing, biological imaging and photodynamic therapy. TrAC Trends in Anal Chem 122:115747
10. Nsengimana B, Khan FA, Awan UA, Wang D, Fang N, Wei W, Zhang W, Ji S (2022) Pseudogenes and liquid phase separation in epigenetic expression. Front Oncol 12:912282
11. Chambers I, Colby D, Robertson M, Nichols J, Lee S, Tweedie S, Smith A (2003) Functional expression cloning of Nanog, a pluripotency sustaining factor in embryonic stem cells. Cell 113(5):643–655
12. Ibrahim EE, Babaei-Jadidi R, Saadeddin A, Spencer-Dene B, Hossaini S, Abuzinadah M (2012) Embryonic NANOG activity defines colorectal cancer stem cells and modulates through AP1- and TCF-dependent mechanisms. Stem cells 30(10):2076–2087
13. Liu B, Badeaux MD, Choy G, Chandra D, Shen I, Jeter CR, Rycaj K, Lee CF, Person MD (2014) Nanog1 in NTERA-2 and recombinant NanogP8 from somatic cancer cells adopt multiple protein

conformations and migrate at multiple MW species. PLoS one 9(3):e90615

14. Kang KT, Shin MJ, Moon HJ, Choi KU, Suh DS, Kim JH (2023) TRRAP enhances cancer stem cell characteristics by regulating NANOG protein stability in colon cancer cells. Int J Mol Sci 24(7):6260. https://doi.org/10.3390/ijms24076260

15. Sneha S, Nagare RP, Manasa P, Vasudevan S, Shabna A, Ganesan TS (2019) Analysis of human stem cell transcription factors. Cell Reprogram 21(4):171–180

16. Zhang L, Hou Y, Lv C, Liu W, Zhang Z, Peng X (2020) Copper-based metal–organic xerogels on paper for chemiluminescence detection of dopamine. Anal Methods 12(34):4191–4198

17. Yang N, Huang Y, Ding G, Fan A (2019) In situ generation of prussian blue with potassium ferrocyanide to improve the sensitivity of chemiluminescence immunoassay using magnetic nanoparticles as label. Anal Chem 91(7):4906–4912

18. Rezaei Z, Ranjbar B (2017) Ultra-sensitive, rapid gold nanoparticle-quantum dot plexcitonic self-assembled aptamer-based nano-biosensor for the detection of human cardiac troponin I. Eng Life Sci 17(2):165–174

19. Shahbazi N, Hosseinkhani S, Ranjbar B (2017) A facile and rapid aptasensor based on split peroxidase DNAzyme for visual detection of carcinoembryonic antigen in saliva. Sens Actuators B: Chem 253:794–803

20. Chen W, Hong L, Liu AL, Liu JQ, Lin XH, Xia XH (2012) Enhanced chemiluminescence of the luminol-hydrogen peroxide system by colloidal cupric oxide nanoparticles as peroxidase mimic. Talanta 99:643–648. https://doi.org/10.1016/j.talanta.2012.06.061

21. Qin G, Zhao S, Huang Y, Jiang J, Ye F (2012) Magnetic bead-sensing-platform-based chemiluminescence resonance energy transfer and its immunoassay application. Anal Chem 84(6):2708–2712. https://doi.org/10.1021/ac202959d

22. Yadav N, Singh A, Kaushik M (2020) Hydrothermal synthesis and characterization of magnetic Fe_3O_4 and APTS coated Fe_3O_4 nanoparticles: physicochemical investigations of interaction with DNA. J Mater Sci: Mater Med 31:1–11

23. Ling W, Wang M, Xiong C, Xie D, Chen Q, Chu X, Qiu X, Li Y, Xiao X (2019) Synthesis, surface modification, and applications of magnetic iron oxide nanoparticles. J Mater Res 34(11):1828–1844

24. Saravanan P, Jayamoorthy K, Anandakumar S (2016) Fluorescence quenching of APTES by Fe2O3 nanoparticles–Sensor and antibacterial applications. J Lumin 178:241–248

25. Chen W, Chen J, Liu AL, Wang LM, Li GW, Lin XH (2011) Peroxidase-like activity of cupric oxide nanoparticle. ChemCatChem 3(7):1151–1154

26. Ehsani M, Chaichi MJ, Nezammeddin Hosseini S (2017) Comparison of CuO nanoparticle and CuO/MWCNT nanocomposite for amplification of chemiluminescence immunoassay for detection of the hepatitis B surface antigen in biological samples. Sensors Actuators B: Chem 247:319–328. https://doi.org/10.1016/j.snb.2017.02.019

27. Shahsavar K, Shokri E, Hosseini M (2022) Sensitive colorimetric detection of miRNA-155 via G-quadruplex DNAzyme decorated spherical nucleic acid. Microchim Acta 189(9):357

28. Naderi M, Hosseini M, Ganjali MR (2018) Naked-eye detection of potassium ions in a novel gold nanoparticle aggregation-based aptasensor. Spectrochim Acta A: Mol Biomol Spectrosc 195:75–83

29. Amani F, TohidiMoghadam T, Farahani N, Ranjbar B (2020) Design and Fabrication of an Aptasensor for Facile and Rapid Detection of Carcinoembryonic Antigen based on Gold-nanoparticles. Modares J Biotechnol 11(2):201–207

30. Mohammadi S, Khajeh K, Taghdir M, Ranjbar B (2021) An experimental investigation on the influence of various buffer concentrations, osmolytes and gold nanoparticles on lysozyme: spectroscopic and calorimetric study. Int J Biol Macromol 172:162–169

31. Barkheh H, Zeinoddini M, Ranjbar B, Xodadadi N (2021) A novel strategy for trinitrotoluene detection using functionalized gold nanoparticles. J Anal Chem 76:459–465

32. Mirsadoughi E, Nemati F, Oroojalian F, Hosseini M (2022) Turn–on FRET-based cysteine sensor by sulfur-doped carbon dots and Au nanoparticles decorated WS2 nanosheet. Spectrochim Acta A: Mol Biomol Spectrosc 272:120903

33. Zhang A, Xiang H, Zhang X, Guo W, Yuan E, Huang C, Jia N (2016) A novel sandwich electrochemiluminescence immunosensor for ultrasensitive detection of carbohydrate antigen 19–9 based on immobilizing luminol on Ag@ BSA core/shell microspheres. Biosens Bioelectron 75:206–212

34. Sam S, Touahir L, Salvador Andresa J, Allongue P, Chazalviel JN, Gouget-Laemmel AC (2010) Semiquantitative study of the EDC/NHS activation of acid terminal groups at modified porous silicon surfaces. Langmuir 26(2):809–814

35. Haghighi AH, Khorasani MT, Faghih Z, Farjadian F (2020) Effects of different quantities of antibody conjugated with magnetic nanoparticles on cell separation efficiency. Heliyon 6(4)

36. Aparna Y, Rao KV, Subbarao PS (2012) Preparation and characterization of CuO Nanoparticles by novel sol-gel technique. J Nano- Electron Phys 4(3):3005–3011

37. Ning X, Bao H, Liu X, Fu H, Wang W, Huang J, Zhang Z (2019) Long-term in vivo CT tracking of mesenchymal stem cells labeled with Au@ BSA@ PLL nanotracers. Nanoscale 11(43):20932–20941

38. Zhang A, Huang C, Shi H, Guo W, Zhang X, Xiang H, Jia T, Miao F, Jia N (2017) Electrochemiluminescence immunosensor for sensitive determination of tumor biomarker CEA based on multifunctionalized Flower-like Au@ BSA nanoparticles. Sens Actuators B: Chem 238:24–31

39. Firoozbakhtian A, Hosseini M, Sheikholeslami MN, Salehnia F, Xu G, Rabbani H, Sobhanie E (2022) Detection of COVID-19: a smartphone-based machine-learning-assisted ECL immunoassay approach with the ability of RT-PCR CT value prediction. Anal Chem 94(47):16361–16368

40. Hosseini M, Sobhanie E, Salehnia F, Xu G, Rabbani H, Sheikholeslami MN, Firoozbakhtian A, Sadeghi N, Farajollah MH, Ganjali MR, Vosough H (2022) Development of sandwich electrochemiluminescence immunosensor for COVID-19 diagnosis by SARS-CoV-2 spike protein detection based on Au@ BSA-luminol nanocomposites. Bioelectrochemistry 147:108161

41. Fuerstenau D (2005) Zeta potentials in the flotation of oxide and silicate minerals. Adv Colloid Interface Sci 114:9–26

42. Chang M-H, Liu H-S, Tai CY (2011) Preparation of copper oxide nanoparticles and its application in nanofluid. Powder Technol 207:378–386

43. Aparna Y, Rao KE, Subbarao PS (2012) Synthesis and characterization of CuO nano particles by novel sol-gel method. In Proc 2nd Int Conf Environ Sci Biotechnol 48:156–160 IACSIT Press Singapore